2016

Analysis on the Performance Limitations of an Interferometric Geolocation Device

Michael Witt
Michigan Technological University, mjwitt@mtu.edu

ANALYSIS ON THE PERFORMANCE LIMITATIONS OF AN INTERFEROMETRIC GEOLOCATION DEVICE

By

Michael J. Witt

A THESIS

Submitted in partial fulfillment of the requirements for the degree of

MASTER OF SCIENCE

In Electrical Engineering

MICHIGAN TECHNOLOGICAL UNIVERSITY

2016

This thesis has been approved in partial fulfillment of the requirements for the Degree of MASTER OF SCIENCE in Electrical Engineering.

Department of Electrical and Computer Engineering

Thesis Advisor:	*Dr. Michael C. Roggemann*
Committee Member:	*Dr. Jeremy Bos*
Committee Member:	*Dr. Timothy Schulz*
Committee Member:	*Dr. Eugene Levin*
Department Chair:	*Dr. Daniel Fuhrmann*

Contents

List of Figures

List of Tables

Abstract

GPS is a critical tool often used in terrestrial location and navigation. However, GPS relies on a system of satellites in medium earth orbit and is prone to dropouts at higher latitudes, and may be susceptible to spoofing or other attacks. Thus, it is prudent to examine possible alternatives. Recently, star tracking has been of interest in global positioning. There are many implementations of a star tracker using an imaging-based optical system to capture star locations in order to estimate position using celestial navigation techniques. These imaging systems are performance limited by blurring imposed by atmospheric turbulence, platform jitter, and measurement noise. An interferometric system for locating stars can be used as an alternative to accurately locate stars in the sky. The use of one or more 3 or 4-aperture interferometers may allow for greater noise immunity in the phase error induced by atmospheric turbulence, and allows a larger baseline to be used as compared to the diameter of a single lens imaging system in some configurations. Such a system could sample at a rate higher than the Greenwood frequency, which helps reduce error in boresight angle retrieval. In the system described herein, the performance limitations would be dominated by atmospheric tilt and boresight angle retrieval. When the boresight angle can be retrieved, the system could be reasonably expected to produce a position estimate RMS error of less than 30 meters.

Chapter 1

Introduction

1.1 Introduction

In acquiring a global position estimate, all that is needed are three fixed reference points and a measurement to those points. In GPS, these references are not fixed, but rather, are on a very precisely known trajectory in orbit around Earth. Measurements to four or more satellites are made, and from this a position estimate is acquired. In a star tracker system, the star-field is assumed to be very accurately known, and given a precise time, the star-field measured can be estimated and overlaid over the known starfield to give an estimate of position[1, 2, 3]. As an application of the van Cittert-Zernike theorem, light from stars could be captured using an interferometric

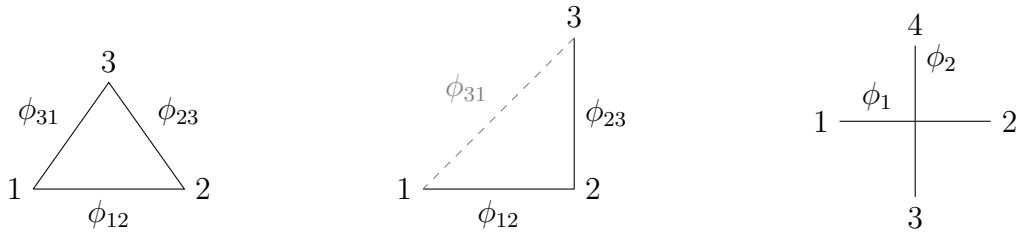

(a) Equilateral Baseline Configuration (b) Orthogonal Baseline Configuration (c) 4-Aperture Baseline Configuration

Figure 1.1: Diagrams of various considered baseline configurations

setup, and rather than imaging a whole star-field, a single star would be imaged and the angle thereto precisely measured[4, 5, 6, 7].

In developing this paper, we considered many different aperture geometries, and while all are fundamentally similar, certain configurations have distinct advantages and disadvantages, discussed in section 1.2. The considered baseline configurations can be seen in Figure 1.1. After much consideration, the configuration chosen for analysis is a 4-aperture configuration, with two independent baselines. Furthermore, three of these setups would be used, each tracking an individual star. A three-aperture interferometer would allow us to measure both azimuth and elevation to an arbitrary star. Similarly, two two-aperture interferometers with noncolinear baselines would allow for the same azimuth and elevation estimates, without needing neutral density filters or beamsplitters. Further constraints are that the device should be somewhat portable, so baselines <1 m are considered, with 4 cm apertures and 1 ms exposure times.

Amplitude interferometry is used here to measure information on a star. If we consider

a 2-aperture interferometer, the fringe pattern disregarding diffraction effects from the aperture is given by[6]

$$I(x) = (I_1 + I_2)\left[1 + \mathscr{V}\cos\left(\frac{2\pi x}{L} + \phi\right)\right] \tag{1.1}$$

where L is the fringe period, and $\mathscr{V}$ is the visibility of the fringe pattern, given by

$$\mathscr{V} = \frac{I_{max} - I_{min}}{I_{max} + I_{min}} \tag{1.2}$$

In this fringe pattern, there are two principal parameters of concern, visibility, $\mathscr{V}$, and phase, ϕ. Following the procedure in Goodman[6], both phase and visibility could be measured as a function of measured photo-electron counts on each detector element. However, while the visibility could be estimated from the measurements, the length of baselines considered herein is small enough that the visibility can reasonably be approximated as 1 when not possible to calculate, but is always close to 1. Furthermore, the only information gained in our setup from estimating the visibility would be an estimate of the angular radius, which is entirely unimportant in this topic. The visibility does play a role in both the fringe and the expected RMS error of the phase estimate, but we can assume that we know the visiblity already since we assume we know which star we are measuring, and referencing a star chart to determine position.

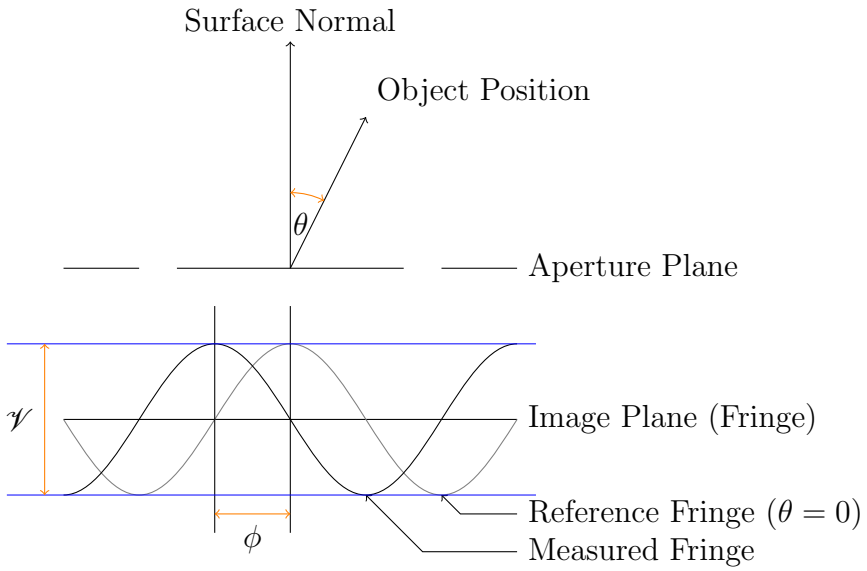

Figure 1.2: Measured fringe relationship with phase offset

Thus, the estimate of ϕ, $\hat{\phi}$ will be the estimator of principal concern, because the phase estimator will be what is used to determine the current location. The phase of (1.1) will be a function of the angular offset from the surface normal, as seen in Figure 1.2. The estimate of the fringe phase gives rise to the estimate of the boresight angle, which in turn generates the position estimate, which will have an RMS error of $r\sigma_\theta$, where r is the radius of the earth and σ_θ is the variance of the boresight angle measurments. This is useful in providing an estimator of the accuracy of the position estimate.

There are two different methods for a physical implementation of a system:

1. The interferometers are mounted to a gimbal, and can be individually directed at stars of interest, which would be selected and approximately located through

the use of a secondary star tracker, one with a large FOV, and the interferometer would have a smaller (around 1 arcminute) FOV. Positioning data from the interferometer could be combined with the gimbal to give accurate star estimates.

2. The interferometer baselines are fixed to a craft or other structure, and the interferometer is designed with a large FOV that is mechanically or electronically restricted to "point" the interferometer at a particular star.

Each configuration has distinct advantages and disadvantages. The first configuration has the advantage of being able to use simpler estimators, although it is at the cost of moving parts. Furthermore, there are physical restrictions to an actual implementation, in that the detector can only be a finite length–if the range of possible boresight angles is large, so must be the detector. Restricting the boresight angles greatly reduces the detector size. The second configuration has the advantage of fewer moving parts, and only requiring one interferometer configuration to obtain an estimate of multiple stars in rapid succession, although the physical size required of the detector may not actually be possible.

For this paper, the first configuration is considered, and it is assumed that the gimbals upon which the interferometers would be mounted can be steered to a much greater accuracy than any of the estimators herein.

1.2 Interferometer concept of operations

Now, we have established that a single baseline pair of apertures in an interferometer will only measure a single angle, as seen in Figure 1.2. Two angles are needed to completely describe a star position in the sky, and so we consider an interferometer with multiple baselines, configured such that both angles to the star can be retrieved.

Then, of importance is discussion of possible aperture geometries. Initially, a three-aperture interferometer was considered, taking one of two possible configurations. The primary concern for such was the potential to use the closure phase, which is much less sensitive to atmospheric turbulence, but still acquire useful azimuth and elevation estimates.

The three baseline configurations considered can be seen in Figure 1.1.

1. A two baseline system requires less complicated optics. The configurations in Figure 1.1a and Figure 1.1b require 1 beamsplitter assuming ϕ_{31} is ignored, or 3 beamsplitters in order to measure ϕ_{31}.

2. The two baseline system in Figure 1.1c captures more light, resulting in a more accurate estimate of the phases. When using the beamsplitters, the number of photons considered in each fringe will need to be at least halved as compared to

the two baseline system. Furthermore, there is an additional aperture, meaning that the two baseline system captures roughly a third more light.

3. The math is greatly simplified. However, this is an advantage only over the configuration in Figure 1.1a, since the math regarding the estimators in Figure 1.1b and c would be the same (with $\phi_{12} = \phi_1$ and $\phi_{23} = \phi_2$), it is nevertheless a reason to discount the configuration in Figure 1.1a.

Therefore, the third configuration, seen in Figure 1.1c, is selected. With the baseline configuration selected, a broader overview of the whole system design to generate a position is necessary. As mentioned in the introduction, it is apparent that multiple references are needed to generate a position estimate. While originally there was some thought that only a single interferometer setup could be used, it has become apparent that this is not the case. The process to generate a position estimate from a single interferometer would be as follows:

1. Determine which star is to be observed, and obtain a general estimate of the position of the star in the sky. This would be accomplished by using an imaging star tracker, since multiple stars would be needed to identify a single star.

2. Point the interferometer at the star.

3. From the measured fringes, determine azimuth and elevation of the star, relative to the interferometer plane. A simple rotational transformation would then be

able to convert this to an azimuth and elevation estimate relative to the horizon.

4. From an accurate time source, calculate sidereal time, and then calculate the 'zenith location' of the star: the location on earth where the star would be directly overhead

5. Consider an arclength s, that is the length of the elevation estimate times the radius of the earth.

6. The position of the interferometer is s away from the zenith location of the star, and is the opposide of the azimuth direction from the zenith location of the star.

This will provide a relatively accurate position of the interferometer, but it starts to fail near the poles of the Earth. Even assuming that magnetic north is known quite accurately (including the location of magnetic north/south), near the poles the accuracy will invariably decrease. Furthermore, near the poles, selection of a star is limited to one of two criteria: either a star is selected that is 'away' from the pole (e.g., if the observation is in the northern hemisphere, a star south of the observer would be selected); or a star is selected whose elevation in the sky, corresponding to the arclength s as defined in the above procedure which in turn corresponds to a circle with radius s, that does not contain the magnetic pole within the circle. These constraints severely limit star selection near the poles, meaning that a star with a sufficient visual magnitude may not be able to be selected.

While the constraints on a single interferometer, two baseline setup do not completely preclude use at the poles, it is worthwhile to consider alternatives. One such alternative is using three of these interferometer setups. Still, only one imaging star tracker would be needed, and the three stars would be selected from within the FOV of the imaging star tracker. Then, each of the three interferometers would be directed to observe one of the three stars selected within the FOV of the star tracker. From the measurements taken by the three interferometers, the elevation could be calculated to each star, which would still correspond to the arclength s. Then, a circle with radius s is centered at each star (with different s for each star), and the intersection of the three circles would give a position estimate. This would still be subject to noise as in the previous cases, but not the constraints on star selection near the poles since azimuth does not play into the position estimate at all.

1.3 Paper organization

The rest of the paper is organized as follows. In Chapter 2, sources of noise in the interferometric fringe pattern measurement are discussed. Section 2.1 discusses the general fringe parameters and relevant parameters. Section 2.2 considers that light is not strictly monochromatic, and introduces a finite bandwidth into the classical fringe. Section 2.3 discusses error as a result of non-zero detector width. Section 2.4 evaluates photon noise in the fringe pattern. Chapter 3 discusses the fringe pattern

relationship with boresight angle, and estimates error in the boresight angle that results from atmospheric effects external to the interferometer. Chapter 4 gives an estimator of position that is useful for comparisons, and develops a comparison to a single aperture imaging system. Section 4.3 concludes the paper.

Chapter 2

Fringe Parameters and Estimation

2.1 Visibility and Phase of a Fringe Pattern

Regardless of the actual fringe pattern, of importance in estimating the phase error will be the visibility $\mathscr{V}$ of the fringe, which is given in (1.2). Considering this, a visibility of 0 will result in the phase of the fringe being irretrievably lost, while a visibility of 1 will yield the best estimate of phase we can expect to obtain. Goodman discusses the phase estimator as the phase of the DFT at the designed spatial frequency. Furthermore, Goodman describes the fringe pattern at a single wavelength in (1.1). Goodman goes on to develop the estimator of ϕ as $\arg(\mathscr{K}(p_0))$, where p_0 is the integer number of fringe periods incident on the detector, and $\mathscr{K}(p)$ is given as

(2.1).[6] Following Goodman, we consider $K(n)$ to be the number of photo-electrons collected by the n-th detector element.

$$\mathscr{K}(p) = \frac{1}{N}\sum_{n=0}^{N-1} K(n)\exp(j2\pi np/N) \tag{2.1}$$

Using this estimator of ϕ, Goodman derives an estimator of the standard deviation of the phase estimator, σ_ϕ, which is given as

$$\sigma_\phi \approx \frac{\sigma_I}{\bar{\mathscr{K}_R}} = \sqrt{\frac{2}{\bar{K}_1 + \bar{K}_2}}\frac{1}{\mathscr{V}} \tag{2.2}$$

We can look at this as being in terms of the number of actual photon counts, which could eventually be useful for determining the accuracy of an actual system, but for now that is not considered. Instead, we use this knowledge, in a later section, to derive the expected accuracy given a star's visual magnitude and angular radius.

Attention is now turned to calculating the visibility of a given star since the visibility will determine, in large part, the SNR of our phase estimate. The visibility of a disk has long since been described[4], as

$$\mathscr{V}(\lambda) = 2\frac{J_1(2\pi\alpha s/\lambda)}{2\pi\alpha s/\lambda} \tag{2.3}$$

where α is the angular radius of the disk, and s is the aperture separation. Then, considering (2.3), it is apparent that larger α will result in a smaller visibility. The

largest angular subtended by a star corresponds to Betelgeuse, and so for various aperture separations that made sense for the system being considered (s between .125 and .75 m), the visibility was calculated for Betelgeuse. This is intended to give a lower bound on the visibility. Furthermore, considering that the wavelength would be in the 900nm range ($\pm$200nm), with a bandwidth of 25 to 100 nm, the mean visibility was seen to always be in the range of .95-1 (although never actually equaling 1), and the visibility within those bandwidths never dropped below .93. This was verified in *Mathematica*, and some of these results can be seen also in Table 2.1, where α was used corresponding to Betelgeuse, which has the largest angular radius on record. This means that these visibilities are absolute worst-case visibilities, since a smaller α will result in a larger visibility. As mentioned earlier, for $s \leq 0.5$ m, the visibilities range from 0.95 to 0.998, and can only be expected to be greater than this for a single star. For separations greater than that, the visibility is still always greater than 0.88, which is still usable, it would only result in a factor of 1.136 larger phase error, as compared to a visibility of 1.

Table 2.1
Various visibilites at given wavelengths assuming $\alpha = 169.7$ nrad, corresponding to the angular radius of Betelgeuse

	Visibility at $\lambda =$				
Seperation (m)	800 nm	850 nm	900 nm	950 nm	1000 nm
0.125	0.997	0.997	0.997	0.998	0.998
0.250	0.986	0.988	0.989	0.990	0.991
0.375	0.969	0.973	0.976	0.978	0.980
0.500	0.946	0.952	0.957	0.961	0.965
0.625	0.916	0.925	0.933	0.940	0.946
0.750	0.880	0.893	0.905	0.914	0.922

2.2 Estimating parameters in the case of finite bandwidth

There was concern that integrating over a finite non-zero bandwidth would be a source of noise, and as such, the following fringe models was developed. The estimate of the fringe at a single wavelength is given by Goodman [6] as (1.1). This fringe was developed by Goodman as a result of considering only a single wavelength. Using the classical equation for L derived from Young's two-slit experiment,

$$L = \frac{\lambda D}{s} \tag{2.4}$$

it is seen that L is a function of wavelength, and when introduced into (1.1), the fringe pattern takes on multiple frequencies. Furthermore, when we consider that the

detector array should be designed such that there are an integer number of periods of fringe over the entire array[6], it is easily seen that this design constraint is not possible given the bandwidth of this function. Therefore, the following fringe pattern was developed, using the standard Fresnel functions "Si" and "Ci", which represent the Sin integral and Cosine integral, respectively, which are given as

$$\mathrm{Si}(x) = \int_0^x \frac{\sin t}{t}\,\mathrm{d}t$$

Similarly, $\mathrm{Ci}(x)$ is defined as:

$$\mathrm{Ci}(x) = -\int_x^\infty \frac{\cos t}{t}\,\mathrm{d}t$$

Next, we integrate (1.1) over a finte bandwidth λ_{bw} centered at λ_c:

$$1 + \frac{\mathscr{V}}{\lambda_{bw}} \int_{\lambda_c - \frac{\lambda_{bw}}{2}}^{\lambda_c + \frac{\lambda_{bw}}{2}} \cos\left(\frac{2\pi x \lambda D}{s} + \phi\right)\,\mathrm{d}\lambda \tag{2.5}$$

Note that this assumes uniform visibility $\mathscr{V}$ over the entire bandwidth of integration. This should not be an issue, as the bandwidth considered for the purposes here is marginal (25-100 nm), but even over the relatively narrow bandwidth, the visibility changes only minimally.

Therefore, given the assumptions so far, we can write the function of the fringe, given

the finite bandwidth λ_{bw} as:

$$f(x) = \frac{1}{2D}\left[4\pi sx\sin(\phi)\mathrm{Ci}\left(\frac{4\pi sx}{2D\lambda + D\lambda_{bw}}\right) - 4\pi sx\sin(\phi)\mathrm{Ci}\left(\frac{4\pi sx}{2D\lambda - D\lambda_{bw}}\right)\right.$$
$$+ 4\pi sx\cos(\phi)\mathrm{Si}\left(\frac{4\pi sx}{2D\lambda + D\lambda_{bw}}\right) - 4\pi sx\cos(\phi)\mathrm{Si}\left(\frac{4\pi sx}{2D\lambda - D\lambda_{bw}}\right) +$$
$$+ 2D\lambda\cos\left(\frac{4\pi sx}{2D\lambda + D\lambda_{bw}} + \phi\right) + D\lambda_{bw}\cos\left(\frac{4\pi sx}{2D\lambda + D\lambda_{bw}} + \phi\right)$$
$$\left. - 2D\lambda\cos\left(\frac{4\pi sx}{2D\lambda - D\lambda_{bw}} + \phi\right) + D\lambda_{bw}\cos\left(\frac{4\pi sx}{2D\lambda - D\lambda_{bw}} + \phi\right)\right] \qquad (2.6)$$

Then, sampling this and taking the FT of the sampled points, we can see that at any reasonable spacing and sample rate, the estimate of ϕ, which is simply the phase of the FT of the sampled points at $p = p_0$ is exactly equal to the actual phase ϕ. This result was verified in Mathematica, simulating the fringe, sampling, then taking the Fourier transform of the sampled points.

2.3 Integration of Fringe Pattern as a result of detector element width

The next source of error considered is the error induced by integrating over the area of a detector element, and then taking each element integration as a sample, and further processing it by taking the Fourier transform of those elements.

Unlike in the previous section, an entirely simulation driven approach was used to evaluate the phase estimate error, to determine if the error is a simply described one, or if it will be a significant source of uncontrollable error.

Mathematica[8] was used to then generate estimated phase error plots, where

$$K(n) = \int_{E_n} f(x)\,\mathrm{d}x \tag{2.7}$$

then $K(n)$ is the integrated intensity of the n-th detector element, and E_n is the x-axis boundaries of the n-th detector element. Of note here is that for this integration, it is important that the elements are indexed properly. If the elements are not indexed properly, then there will be a constant offset in the phase error, in addition to the error shown in Figure 2.1. The mean error can be accounted for however, as the error is only a function of the design parameters of the interferometer, which are closely known. Thus, we consider the phase error to be $E_\phi[\hat{\phi} - \phi] - E[E_\phi[\hat{\phi} - \phi]]$, or the expected error of the estimator minus the DC offset; which further assumes that the estimate of the phase, $\hat{\phi}$ will be uniformly distributed.

However, even without considering the limitations and prior knowledge of ϕ, the range of error, for a reasonable set of design parameters, is only on the order of tens of microradians. As demonstrated in section 2.4, we see that this source of error will be very much overpowered by photon noise. As such, this source of error is neglected.

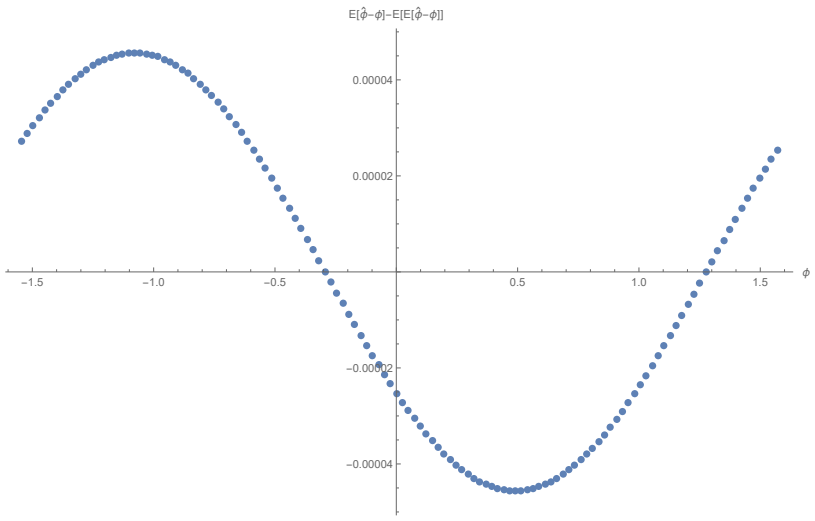

Figure 2.1: Phase error $(E[\hat{\phi} - \phi] - E[E[\hat{\phi} - \phi]])$ vs. ϕ; $\bar{\lambda} = 900$nm, $\lambda_{bw} = 50$nm, 512 samples, $p_0 = 10$

2.4 Photon Noise Limits

The last consideration for estimating the error in the phase estimate is the noise induced by photon noise. That is, the error as a result of there being an integer number of photo-events on each detector element, a finite number of photo-events occurring over the entire detector element, and a random number of photo-events occuring on the detector from exposure to exposure.

Using code provided by Dr. Roggemann[9] which was converted for use in Mathematica, visual magnitudes, in conjunction with assumed aperture dimensions, were used to generate real, expected photon counts[8, 10].

Goodman has done a thorough job of investigating photon noise in such an interferometer[6], but uses his own notation, using the terms $\bar{K}_i = \alpha N\, A\tau I_i$ with $\alpha = \frac{h\bar{\nu}}{\eta}$, where η is the quantum efficiency, h is Planck's constant, and $\bar{\nu}$ is the mean frequency of analysis. Therefore, we can see quite simply that $\bar{K}_i$ is the expected mean photon count over all detector elements arising from the i-th aperture. Therefore, a logical extension to this is to use visual magnitudes to directly calculate photon counts[8, 9]. Furthermore, the code provided in `vmag_sub.m` takes into account lens and atmospheric transmission, as well as quantum efficiency, as in the equations considered by Goodman. As such, the photon counts produced by said code can easily be said to be equivalent to $\bar{K}_i$. Also extending this is the assumption that all intensities incident on the apertures are going to be equal; which is not unreasonable since all apertures in the considered interferometer will have the same physical characteristics and all will be directed at the same star. Given these assumptions, we can rewrite σ_ϕ as

$$\sigma_\phi = \sqrt{\frac{1}{\text{Photon Count}}}\frac{1}{\cancel{\mathscr{V}}} \tag{2.8}$$

Evaluating σ_ϕ for various visual magnitudes in Mathematica, we obtain Table 2.

From the sample data, we see that in a best case scenario, we have errors on the order of 6-15 millirad. In Section 4.1 we will discuss how those errors relate to position estimate errors.

Table 2.2
RMS Error and magnitudes for sample stars, $\eta = 0.95, \tau = 1$ ms

Star	Sun	Sirius	Canopus	Arcturus	Rigel Kentarus A	Vega	Capella	Rigel
Vmag	-26.72	-1.44	-0.62	-0.05	-0.01	0.03	0.08	0.18
Error	0.03476	0.006591	0.009615	0.01252	0.01273	0.01297	0.01327	0.01390

Chapter 3

Boresight Angle Measurement and Noise

3.1 Retrieving boresight angle from phase information

As mentioned in the introduction, the phase angle, ϕ in (1.1) is a function of what will be called the 'boresight angle' or, the angle from the surface normal of the interferometer to the source. If we consider that the boresight angle is θ, aperture separation s, and focal length D, then an expression for ϕ–the phase angle–can be derived, using one of two different approaches

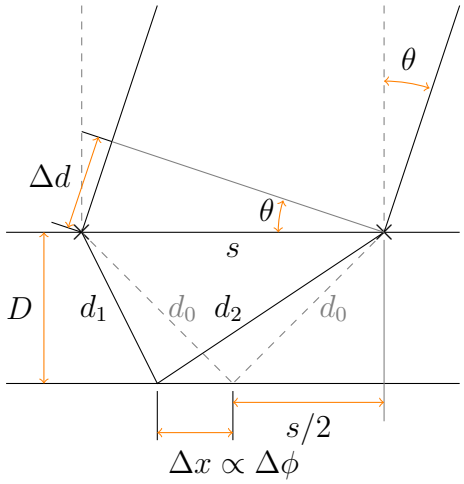

Figure 3.1: Illustration of relationship of measured phase ($\Delta\phi$) and bore-sight angle (θ)

3.1.1 Geometric optics approach

First, let $\theta = 0$. Then, there will be maxima where the path lengths are both multiples of the wavelength. Considering this, there should be a maximum where the path lengths are equal. Now, consider the length from each aperture to the detector plane to be length d_0, and the lengths from each aperture to the detector plane are equal because $\theta = 0$. Now, consider the source is moved off-axis by θ. The new location on the detector plane is given by forming a triangle, with length d_1 from one aperture, and d_2 from the second aperture. Since we are concerned with the same maximum moving, and we are considering the maximum where the path lengths are equal, we can introduce a length Δd, which describes the difference in path length, $d_2 - d_1$. Using geometric identities, it can be shown that $\Delta d = d_2 - d_1 = s \sin\theta$. Finally, we consider the point where this maximum occurs to have moved by Δx,

which will later be shown to be proportional to $\Delta\phi$. These principles are illustrated in Figure 3.1. Given these constraints:

$$d_2 = d_1 - s\sin\theta \tag{3.1}$$

$$d_1 = \sqrt{D^2 + \left(\frac{s}{2} + \Delta x\right)^2} \tag{3.2}$$

$$d_2^2 = D^2 + \left(\frac{s}{2} - \Delta x\right)^2 \tag{3.3}$$

substituting (3.1) into (3.3)

$$(d_1 - s\sin\theta)^2 = D^2 + \left(\frac{s}{2} - \Delta x\right)^2 \tag{3.4}$$

then substituting (3.2) into (3.4)

$$\left(\sqrt{D^2 + \left(\frac{s}{2} + \Delta x\right)^2} - s\sin\theta\right)^2 = D^2 + \left(\frac{s}{2} - \Delta x\right)^2 \tag{3.5}$$

solving for Δx

$$\Delta x = \begin{cases} -\frac{\sqrt{4D^2\sin^2(\theta) - s^2\sin^4(\theta) + s^2\sin^2(\theta)}}{2\sqrt{1-\sin^2(\theta)}} & \theta < 0 \\ \frac{\sqrt{4D^2\sin^2(\theta) - s^2\sin^4(\theta) + s^2\sin^2(\theta)}}{2\sqrt{1-\sin^2(\theta)}} & \theta \geq 0 \end{cases} \tag{3.6}$$

Now that the expression for Δx has been obtained, the relationship with $\Delta\phi$ is

$$\Delta\phi = 2\pi\frac{\Delta x}{L} \tag{3.7}$$

where L is the fringe spacing given in (2.4). Then, substituting (3.6) into (3.7), we obtain

$$\Delta\phi = \begin{cases} -\frac{2\pi}{L}\frac{\sqrt{4D^2\sin^2(\theta)-s^2\sin^4(\theta)+s^2\sin^2(\theta)}}{2\sqrt{1-\sin^2(\theta)}} & \theta < 0 \\ \frac{2\pi}{L}\frac{\sqrt{4D^2\sin^2(\theta)-s^2\sin^4(\theta)+s^2\sin^2(\theta)}}{2\sqrt{1-\sin^2(\theta)}} & \theta \geq 0 \end{cases} \tag{3.8}$$

Then, since ϕ is measured, and θ is the desired quantity, we solve (3.8) for θ:

$$\theta = \begin{cases} \arcsin\left(\frac{\sqrt{\frac{-\sqrt{(\pi^2(4D^2+s^2)+\Delta\phi^2L^2)^2-4\pi^2\Delta\phi^2L^2s^2}+\pi^2(4D^2+s^2)+\Delta\phi^2L^2}{s^2}}}{\sqrt{2}\pi}\right) & \Delta\phi \geq 0 \\ -\arcsin\left(\frac{\sqrt{\frac{-\sqrt{(\pi^2(4D^2+s^2)+\Delta\phi^2L^2)^2-4\pi^2\Delta\phi^2L^2s^2}+\pi^2(4D^2+s^2)+\Delta\phi^2L^2}{s^2}}}{\sqrt{2}\pi}\right) & \Delta\phi < 0 \end{cases} \tag{3.9}$$

If we consider that the boresight should be nominally pointed at the star, to within approximately one arcminute (or approximately 300 microradians), we can use the small angle approximation for this, and expect an error no greater than 1%, which is significantly less than other sources of error

$$\theta \approx \frac{\sqrt{\frac{-\sqrt{(\pi^2(4D^2+s^2)+\Delta\phi^2L^2)^2-4\pi^2\Delta\phi^2L^2s^2}+\pi^2(4D^2+s^2)+\Delta\phi^2L^2}{s^2}}}{\sqrt{2}\pi} \times \begin{cases} 1 & \Delta\phi \geq 0 \\ -1 & \Delta\phi < 0 \end{cases} \tag{3.10}$$

3.1.2 Fourier Optics Approach

If we instead want to consider an expression for ϕ that does not require use of the focal length or period of the fringe pattern, a Fourier optics approach can be used. Instead of considering the fringe pattern moving on the detector, it is considered that we can treat the measured phase of the fringe pattern as the phase of the Fourier transform at a specific spatial frequency [6].

For the sake of this treatment, we express our fringe pattern as a complex visibility, which will be denoted as $\mathbb{V}$. Then,

$$\mathbb{V} = \mathscr{V} e^{-j\phi} \tag{3.11}$$

Now, considering that we are looking at a single star in the object space, at some angles θ_x and θ_y being the zenith angles along the x and y axes respectively, with r representing the distance to the object plane or star in this case.

$$f(x, y) = \delta(x - r\tan\theta_x, y - \tan\theta_y) \tag{3.12}$$

We can take the Fourier transform of this function to be

$$F(u, v) = \exp(j2\pi r(u\tan\theta_x + v\tan\theta_y)) \tag{3.13}$$

We now consider our interferometers to measure at the spatial frequency f_s

$$f_s = \frac{\vec{s}}{\lambda r} \tag{3.14}$$

where $\vec{s}$ is a vector describing the length and orientation of the interferometer baseline. Then, evauluating for orthogonal baselines oriented along the x and y axes:

$$\mathbb{V}_x = F\left(\frac{s}{\lambda r}, 0\right), \mathbb{V}_y = F\left(0, \frac{s}{\lambda r}\right) \tag{3.15}$$

and finding ϕ_i corresponding to $\mathbb{V}_x$ and $\mathbb{V}_y$,

$$\phi_i = \frac{2\pi s \tan\theta_i}{\lambda} \tag{3.16}$$

However, since ϕ_i is the argument of an exponential, we will only be able to measure it modulo 2π. We see this same problem arise whether we use a geometric optics approach as in the previous section, or the Fourier optics approach seen in this section.

3.1.3 Problems in boresight angle retrieval

While there is clearly an inverse function for θ, the range of that inverse function is quite limited, owing to the fact that ϕ can only be measured to within a 2π range through the Fourier estimate discussed in section 3. As an example, we'll let $D = s =$

0.5 m $\implies$ $L = \lambda = 900 \times 10^{-9}$ m. Then, for $\Delta\phi = 2\pi$, $\theta = 1.8 \times 10^{-6}$ rad, or less than half an arcsecond. The problem is that the interferometer reading is supposed to refine the position estimate of the star in question: but this would require knowledge of the star location to less than half an arcsecond. If that was already known, a position estimate accurate to roughly 15 meters could be obtained.

This is not impossible to compensate for, however. While the fringe pattern is given in (1.1), there are a couple of effects that could be exploited. The simplest effect is driven by the Fourier optics approach, where we pick two different baseline lengths which ideally should have a very large lowest common multiple. Then, assuming the baselines are concentric and oriented the same, we can generate a table of values for each baseline that correspond to possible boresight angles. Then, for each baseline, we write the possible boresight angles as the sum of a set of Dirac delta functions, which is then convolved with a likelihood function, ideally corresponding to the measurement noise. Then, the product of the two separate baseline likelihood functions could be maximized to produce an ML estimate of the true boresight angle.

Another approach could be to exploit a diffraction pattern, which can be described as an envelope on the fringe pattern. If we select a square aperture, it is known that the diffraction pattern will be a sinc function. Then, since the sinc function should have a larger period than the fringe pattern, a Fourier transform could give us an estimate of the phase, and therefore location of the maximum of the diffraction

pattern. Alternatively, if the diffraction pattern is simply known and not necessarily a sinc function, a fit could be attempted to fit the envelope to the data, also providing more information about the boresight angle.

Finally, the third approach considers that the fringe pattern derived in (2.6) is nominally a sin function, with a sinc-like envelope. This corresponds similarly to how it was defined in the first place, as the integral over a uniformally distributed sin function at multiple wavelengths; in the Fourier domain it would be similar to a rect function in the frequency domain that is not centered at zero being inverse Fourier transformed. Therefore, if the period of the sinc 'envelope' that arises from finite bandwidth could be calculated, the Fourier phase of the envelope could give information as to the true boresight angle.

3.2 Atmospheric Effects

3.2.1 Fringe Jitter

Of concern is that the tilt from atmospheric turbulence will produce a noticeable error in the measured boresight angle. This type of tilt jitter has been discussed

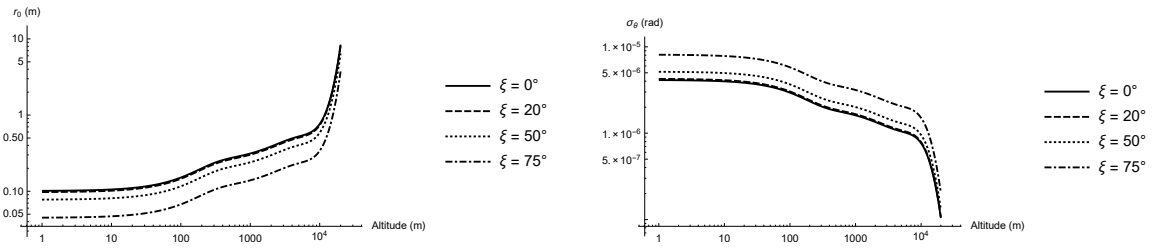

Calculated r_0 Calculated σ_θ

Figure 3.2: Calculated r_0 and σ_θ for various zenith angles (ξ)

previously[7, 11], and the phase error will be given by

$$\sigma_\theta = \sqrt{0.170 \left(\frac{\lambda}{D}\right)^2 \left(\frac{D}{r_0}\right)^{5/3}} \tag{3.17}$$

We consider σ_θ to be given in radians.

(3.17) is quite straightforward to evaluate, although in order to do so, a value for r_0 needs to be calculated, which is not as trivial. For this purpose, the H-$V_{5/7}$ model is used[5], corresponding to moderate turbulence in the atmosphere. This is then combined with (3.17), and calculated for various zenith angles (on which r_0 is dependent).

3.2.2 Refraction

For any elevation measurement deviating significantly from the zenith angle, there will be a non-negligible amount of refraction that occurs. This however is well known, and the true zenith angle can be computed to within 150mas using the procedure

outlined by Stone[12].

3.2.3 Atmospheric Time Constant

There is another limitation imposed by the atmosphere, described by the Greenwood frequency, which is essentially the maximum frequency at which the atmosphere changes. While this will not contribute to noise, if higher precision is desired in the position estimate, a trivial solution would be to average multiple position estimates. Furthermore, if we consider that the exposure time considered herein is 1ms, then it would seem that 1000 samples could be averaged over a second to reduce the positioning error. However, the tilt imposed by the atmosphere on a star measurement is correlated in time, therefore two successive measurements will have a certain amount of correlation. The maximum frequency at which the star could be sampled and expect the atmospheric effects to be different is given by the Greenwood frequency. The inverse of the Greenwood frequency can then be seen to give us an estimate of how rapidly we can sample a star and assume different boresight measurements, also called the Greenwood time constant. We will use a simplified form of the Greenwood time constant which assumes a uniform windspeed[5]

$$\tau_0 = \frac{0.32 r_0}{v} \tag{3.18}$$

where v is the wind speed. We already have calculated r_0 above, and we will assume the wind speed is 21 m/s, as in the H-$V_{5/7}$ model, This results in, at sea level, a time constant of roughly 1.5 ms. While not a large limitation, it is clear that fewer samples would be able to be averaged over a second, and because r_0 increases as height increases, fewer samples would be able to be averaged as the altitude of the observer increases.

3.3 Azimuth and Elevation Estimates

The two baselines now give us two measurements of an angle to the boresight, which are referred to as the boresight angles. As discussed earlier, we consider one baseline along the x-axis, and one baseline along the y-axis. Then, the star in consideration is on the plane defined by the three points $(0,0,0), (0,1,0), (\cos 90^\circ - \theta_x, 0, \sin 90^\circ - \theta_x)$ where θ_x is the measured boresight angle. Now, consider the general equation for a plane:

$$\mathbf{n} \cdot (x - x_0, y - y_0, z - z_0) = 0 \tag{3.19}$$

where $\mathbf{n}$ is the surface normal vector, and (x_0, y_0, z_0) is a point on the plane. Then, from the earlier definition, we select $(0,0,0)$ for the point on the plane, and the surface

normal will be

$$\mathbf{n} = (\cos 90^\circ - \theta_x, 0, \sin 90^\circ - \theta_x) \times (0, 1, 0) = (\cos \theta_x, 0, -\sin \theta_x) \tag{3.20}$$

therefore the equation of the plane will be

$$x \cos \theta_x - z \sin \theta_x = 0 \tag{3.21}$$

Following the same procedure for the y-axis baseline, the equation for the plane will be

$$-y \cos \theta_y + z \sin \theta_y = 0 \tag{3.22}$$

If we were to solve these two equations as a system of equations, we would obtain an equation for a line through the origin. If we let there be a sphere, such that the radius of the sphere is 1, then we can write the equation for the surface of a sphere as

$$\sqrt{x^2 + y^2 + z^2} = 1 \tag{3.23}$$

Then, we solve the system of equations:

$$\begin{cases} x \cos \theta_x - z \sin \theta_x = 0 \\ -y \cos \theta_y + z \sin \theta_y = 0 \\ \sqrt{x^2 + y^2 + z^2} = 1 \end{cases} \tag{3.24}$$

We obtain:

$$\begin{cases} x = \frac{\sin(\theta_x)\cos(\theta_y)}{\sqrt{\cos^2(\theta_x)\cos^2(\theta_y)+\sin^2(\theta_x)\cos^2(\theta_y)+\cos^2(\theta_x)\sin^2(\theta_y)}} \\ y = \frac{\cos(\theta_x)\sin(\theta_y)}{\sqrt{\cos^2(\theta_x)\cos^2(\theta_y)+\sin^2(\theta_x)\cos^2(\theta_y)+\cos^2(\theta_x)\sin^2(\theta_y)}} \\ z = \frac{\cos(\theta_x)\cos(\theta_y)}{\sqrt{\cos^2(\theta_x)\cos^2(\theta_y)+\sin^2(\theta_x)\cos^2(\theta_y)+\cos^2(\theta_x)\sin^2(\theta_y)}} \end{cases} \tag{3.25}$$

after discarding the negative z solution, since the star observed can not be below the interferometer plane.

Now, we can convert to spherical coordinates in the form (r, ξ, ψ), where ξ will be the azimuth angle with respect to the x axis, and ψ will be the boresight angle, i.e. θ in Figure 1.2. These coordinates are given as[13]

$$\begin{cases} r = \sqrt{x^2 + y^2 + z^2} \\ \xi = \arctan\frac{y}{x} \\ \psi = \arccos\frac{z}{r} \end{cases} \tag{3.26}$$

We can substitute our found equations into this system, and simplifying using Mathematica:

$$\begin{cases} r = 1 \\ \xi = \arctan(\cot(\theta_x)\tan(\theta_y)) \\ \psi = \arccos\left(\frac{\cos(\theta_x)\cos(\theta_y)}{\sqrt{\sin^2(\theta_x)\cos^2(\theta_y)+\cos^2(\theta_x)}}\right) \end{cases} \tag{3.27}$$

As expected, since we let the radius of the sphere be equal to 1 in (3.24), we obtain

$r = 1$ in this form as well. From this, a simple rotation is all that is needed to convert this to azimuth with respect to north and zenith angle.

Chapter 4

Results and Conclusion

4.1 Position Estimation

Attention is now turned to position estimation. It is considered that we now have a zenith angle estimate to each of three stars, with some RMS error σ_{zi} relative to the i-th star.

First, we consider that the interferometer is pointed at a given star, and that the given star is already identified. Then, we can use a standard star map, such as J2000, to look up the right ascension and declination of a given star. From this and an accurate time source, we can calculate a 'zenith location' of the star, which is a location on Earth where the star is at zenith or directly overhead. Then, we can use our measured

zenith angle to calculate an arclength s to the star. This arclength is shortened based on the elevation of the observer, which is assumed to be very precisely known. We then consider that our actual position lies on a locus of points distance s away from the zenith location of the star. We incorporate σ_{zi} by considering it as a width either side of our locus of points, creating a Gaussian profile with the peak at exactly s away from the zenith location. Then, two more loci are generated in the same procedure. Finally, the product of the three locus profiles is generated, and the location of the maximum is taken to be the position.

Before this estimator is derived, we will consider that this may not be an optimal estimator; rather, it is intended to give an idea of the lower bounds of performance for the use of an interferometer in determining position. In fact, we know that this is a suboptimal estimator since we are immediately discarding information in the form of the azimuth estimate, and only concerning ourselves with the zenith angle estimate. Furthermore, we will derive this math on a plane, rather than on the surface of a sphere. This should give us a reasonable approximation to the actual case wherein the coordinates will lie on a sphere, owing to the fact that in selecting a star, we should choose stars that are no more than about 20° away from zenith, and therefore should all have relatively close zenith locations. This also greatly simplifies the math.

First, let us calculate the zenith location of a star, the location on Earth where the star is directly at zenith. This calculation is quite trivial. Consider that the right ascension

and declination is precisely known. Then, also assume that the sidereal time is also known, and is quite accurate. Then, the latitude of the zenith location will be the declination, and the longitude will be the right ascension minus the current sidereal time. Of course, in this estimate the latitude will be known to a very precise value, as declination and right ascension have been measured to within miliarcseconds, and sidereal time will be accurate to approximately the same accuracy as a clock, which should yield sub-second accuracy, and consequently, sub-arcsecond accuracy in angle measurement. We will consider this zenith location to be at the point (x_0, y_0).

Now, let us consider the zenith angle measurement, θ, which has an expected RMS error of σ_θ. Then, we can consider that this gives an estimate of the distance to the zenith location, by considering an arclength s, where $s = r\theta$ and r is the radius of the Earth. Then, the locus of points that is s away from the zenith location can be given by the equation for a circle, $s^2 = (x - x_0)^2 + (y - y_0)^2$. Now, we can consider that this circle will be in error by $\sigma_{xy} = r\sigma_\theta$. Continuing this line of reasoning, we can describe the likelihood function along this locus of points as

$$f(x, y) = \frac{1}{\sigma_{xy}} \exp\left(-\frac{\left(\sqrt{(x - x_0)^2 + (y - y_0)^2} - s\right)^2}{2\sigma_{xy}^2} \right) \tag{4.1}$$

We can now consider this for various stars and arclengths. If we consider that the boresight angle can be retrieved, then the noise will be dominated by atmospheric tilt–as the G-tilt discussed previously–and we consider a σ_θ corresponding to a worst

case scenario seen in the G-tilt discussion, or 5 microradians, and the radius of Earth being 6370 km, then we can set up a simulation to test the accuracy of our position estimator. This is simulated rather than calculated analytically since there are multiple nonlinear functions of multiple Gaussian random variables; although we see later that the resulting position estimates can be reasonably seen to be Gaussian.

The process is as follows:

1. Select 3 zenith locations on a plane, as well as our current position. This is where our generated stars will be, and for simplicity, we select our position to be at $(0, 0)$.

2. From the star zenith locations, calculate a corresponding 'actual' zenith angle, which is the distance from our position to the star zenith location, divided by the radius of Earth.

3. Introduce noise into this zenith angle, which will correspond to our measured zenith angle. This introduced noise is characterized by σ_θ, being zero-mean Gaussian.

4. Generate arclengths from star measurements

5. Generate ML estimate of position from zenith locations of stars and measured distances.

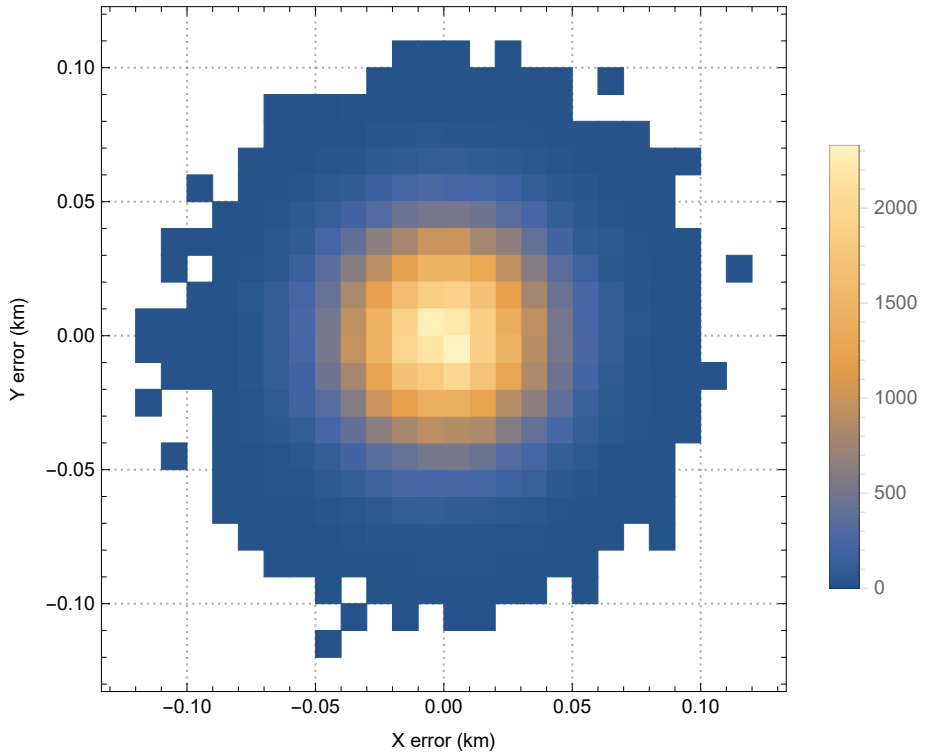

Figure 4.1: ML position error density histogram, 100000 samples

When running this simulation, we can obtain a density histogram, an example seen in Figure 4.1. We might expect that, for a 5 microradian error in boresight angle measurement, we would see an error just less than 31 meters. The simulation resulted in position errors in arbitrary orthogonal directions of roughly 26 meters, and we also can show that they can be modeled as Gaussian, using the Cramer-von Mises test, to a 95% confidence level, in this simulated example.

4.2 Comparison to Single-Aperture Systems

Of concern in describing a system such as this three or four aperture interferometric system is comparing the system to a similar single-aperture imaging star-tracker. While there are many papers on the subject in determining orbital attitude, very few exist that are designed to work within the atmosphere, and none with published performance specifications. Therefore we will consider a theoretical model of such a system, and explain why the interferometric system outperforms an equivalent single-aperture system.

Fried has discussed, in-depth, the resolution limits imposed by atmospheric turbulence. Furthermore, he has considered the resolution limits imposed by the atmosphere, as well as near-field and far-field; with short and long exposure lengths, although with long exposure lengths, near-field or far-field becomes irrelevant[14]. From his research, the optimal exposure is near-field, short exposure; then far-field, short exposure; and finally long exposure. The interferometer clearly falls within the far-field, short exposure category, with exposure times of 1ms selected herein. Therefore the PSF of the interferometric exposure is quite narrow, although the system will be exposed to tip and tilt which will vary the measurement. By comparison, the traditional imaging star tracker will likely need to use a longer exposure time, which is not suitable for use within the atmosphere for reasons that will be discussed here.

One difficulty in comparing an imaging star tracker to the proposed interferometric setup is the vast number of parameters that need to be optimized for a specific application. In an environment outside of the atmosphere, a long exposure time is a reasonable design consideration, but not as practical inside of the atmosphere, but may be necessary.

In selecting exposure time for an imaging tracker, there are two primary considerations:

1. Atmospheric effects will increase the angular extent of the star as the exposure time increases, to a limit,

2. Blurred image processing recommends a higher number of photoelectrons to increase accuracy

The first consideration implies that the shortest practical exposure time should be used, ideally in the millisecond range, but the second constraint requires a longer exposure time. This is, of course, without even considering other effects that may need to be mitigated, such as platform vibration or motion.

To calculate the accuracy of a comparable star tracker, the previously calculated photoelectron counts can be used, which would give a reasonable approximation of an imaging tracker that has similar characteristics. Then, using the NEA, or Noise

Angle Approximation by Leibe[2], we can describe the accuracy as

$$NEA = \frac{FOV \times E_{centroid}}{N_{pixel} \times \sqrt{N_{star}}} \tag{4.2}$$

FOV is the field of view for a star tracker. For our purposes, we'll consider a 20° FOV. N_{pixel} is the number of pixels on a side of the detector; 256-1024 seems to be a fairly common range in the literature[1, 2, 3], and so we chose 512 pixels. N_{star} is the number of stars used in centroiding; we select 20 stars. Finally, $E_{centroid}$ is the subpixel accuracy of the centroiding algorithm, and we will include other noise effects in this term. Within the atmosphere, we can include in $E_{centroid}$ the tilt imposed by the atmosphere. Using our previous expression for G-Tilt, and since we are assuming a 5 cm aperture, we can calculate a worst case tilt of about 10 microradians[11]. To convert this to the pixel accuracy that $E_{centroid}$ is already in, we can use the expression

$$\frac{\sigma_\theta}{FOV} N_{pixel} \tag{4.3}$$

which gives us about 0.0144 pixels. Using our previously calculated photoelectron counts, which we will say is roughly 1000-10000, we expect $E_{centroid}$ from only the centroiding algorithm to be around 0.1 pixel. We can then add these two values together, and calculate out our value for the NEA. Using these parameters, we get an accuracy of about 0.001°, which, when we multiply by the radius of the Earth, would give us an accuracy of about 111.3 m.

4.3 Conclusion

This paper has discussed how an interferomteric system to generate global positioning information might work, and detailed what the major performance limitations should be. For this paper, the primary consideration is that any such interferometric system should be relatively portable, so a baseline around half a meter was considered. Exposure times were also deliberately selected such that we could reasonably treat atmospheric turbulence as being frozen. Given these constraints, we constructed a model for the fringe pattern given finite bandwidth; constructed a model for measuring error induced by finite detector element width; and finally photon noise. Then, using these error metrics, we constructed a potential method for retrieving the boresight angle. Finally, we constructed one estimator of position using three star measurements to give us a reasonable bound on performance. In order to gauge the performance of a potential interferometric system, a simple blurred image processing star tracker was modeled, using similar constraints to that of the interferometric implementation. We found that under similar exposure times and single aperture sizes, we could expect a single exposure accuracy from the interferometric system to be on the order of 25-30 meters, while the single aperture imaging star tracker would provide an accuracy of around 110 meters. Also considered was that even the single exposure performance would likely need to be improved, for either system, and so the Greenwood frequency was discussed as placing a maximum on the exposure rate.

References

[1] Shuster, M. D. and Oh, S. D., "Three-axis attitude determination from vector observations," *J. Guidance and Control* **4**, 70–77 (February 1981).

[2] Liebe, C. C., "Accuracy performance of star trackers–a tutorial," *IEEE Transactions on Aerospace and Electronic Systems* **38**, 587–599 (April 2002). 2002.

[3] [*A Star Tracker Design for CubeSats*] (2012).

[4] Steel, W. H., [*Interferometry*], Cambridge University Press (1967).

[5] Larry C. Andrews, R. L. P., [*Laser Beam Propogation through Random Media*], SPIE Press, second ed. (2005).

[6] Goodman, J. W., [*Statistical Optics*], Wiley-Interscience, first ed. (1985).

[7] Glindemann, A., [*Principles of Stellar Interferometry*], Springer (2011).

[8] Inc., W. R., [*Mathematica*], Wolfram Research, Inc., version 10.2 ed. (2015).

[9] Roggemann, M. C., "`vmag_sub.m`." MATLAB Code.

[10] Roggemann, M. C., "Photon-noise limits to the detection of the closure phase in optical interferometry," *Applied Optics* **35**, 1809–1814 (April 1996).

[11] Tyler, G. A., "Bandwidth considerations for tracking through turbulence," *Journal of the Optical Society of America A, Optics and Image Science* **11**, 358–367 (January 1994).

[12] Stone, R. C., "An accurate method for computing atmospheric refraction," *Publications of the Astronomical Society of the Pacific* **108**, 1051–1058 (November 1996).

[13] Weisstein, E. W., "Spherical coordinates." From MathWorld–A Wolfram Web Resource. http://mathworld.wolfram.com/SphericalCoordinates.html.

[14] Fried, D. L., "Optical resolution through a random inhomogenous medium for very long and very short exposures," *Journal of the Optical Society of America* **56**, 1372–1379 (October 1966).

[15] Cornwell, T. J., "The applications of closure phase to astronomical imaging," *Science* **245**, 263–269 (July 1989).

[16] Goodman, J. W., [*Fourier Optics*], Roberts & Company, third ed. (2005).

[17] Harry L. Van Trees, Kristine L. Bell, Z. T., [*Detection, Estimation, and Modulation Theory*], vol. Part I - Detection, Estimation, and Filtering Theory, Wiley, second ed. (2013).

[18] Kay, S. M., [*Fundamentals of Statistical Signal Processing*], vol. Volume I - Estimation Theory of *Prentice Hall Signal Processing Series*, Prentice Hall PTR (1993).